Mechanics of Advanced Materials and Structures, 12:331–340, 2005

ISSN: 1537-6494 print / 1537-6532 online
DOI: 10.1080/15376490500182057

Taylor & Francis
Taylor & Francis Group

Equivalent Single-Layer and Layerwise Shell Theories and Rigid-Body Motions—Part II: Computational Aspects

G. M. Kulikov and S. V. Plotnikova
Department of Applied Mathematics and Mechanics, Tambov State Technical University, Tambov, Russia

The precise representation of rigid-body motions in the displacement patterns of the first-order equivalent single-layer (ESL) and layer-wise (LW) shell elements has been considered in the companion paper (Part I). In this paper, computational aspects of the ESL shell formulation are discussed in detail. To overcome shear and membrane locking and have no spurious zero energy modes, the assumed strain and stress resultant fields are invoked. On the basis of this approach, a family of four-node *curved* ESL shell elements is designed. All elemental stiffness matrices have six, and only six, zero eigenvalues and require only direct substitutions. Besides, they are evaluated by using the full exact *analytical* integration. To demonstrate the efficiency and accuracy of the developed formulation, extensive numerical studies are presented.

§1. INTRODUCTION

It is common knowledge when an inconsistent (in the sense of the adequate representation of rigid-body motions) shell theory is used to construct any finite element, erroneous straining modes under rigid-body motions may appear. This problem has been studied for the equivalent single-layer (ESL) and layer-wise (LW) shell theories in authors' companion paper [1]. Herein, we address in detail the computational aspects of the ESL shell theory. The proposed finite element formulation is based on the simple and efficient approximation of shells via four-node *curved* shell elements. To avoid shear and membrane locking, and to have no spurious zero energy modes, the assumed stress resultant and displacement-independent strain fields are invoked. This approach was proposed by Wempner et al. [2] for the geometrically linear first-order shear deformation shell theory and further was developed for the Timoshenko beam, Mindlin plate, and Timoshenko-Mindlin-type shell theories [3–6] with account for the transverse normal deformation response.

Received 20 January 2005; accepted 20 January 2005.
This research was supported by Russian Fund of Basic Research (Grant no. 04-01-00070).
Address correspondence to Prof. G. M. Kulikov, Department of Applied Mathematics and Mechanics, Tambov State Technical University, Sovetskaya Street 106, Tambov 392000, Russia. E-mail: kulikov@apmath.tstu.ru

On the basis of this formulation, a family of four-node *curved* ESL shell elements is designed. One of them is too stiff because thickness locking occurs. The other three ESL shell elements demonstrate an excellent performance for the thin-walled composite structures. It is remarkable that all constructed elemental stiffness matrices have six, and only six, zero eigenvalues as required for satisfaction of the general rigid-body motion representation. Besides, our stiffness matrices require only direct substitutions, that is, no inversion is needed if sides of the element coincide with lines of principal curvatures of the reference surface, and they are evaluated by using the 3D *analytical* integration. So, our finite element formulation is very economical and efficient compared to the conventional isoparametric finite element formulations because it reduces the costly numerical integration by deriving the elemental stiffness matrices [7, 8]. To demonstrate the efficiency and high accuracy of the developed ESL and LW shell formulations, extensive analytical and numerical studies are presented.

§2. FINITE ELEMENT FORMULATION

In order to develop the finite element ESL shell formulation, we write the mixed variational Eq. (26) from work [1] for the shell element as follows:

$$\int_{-1}^{1}\int_{-1}^{1}[\delta\mathbf{E}^{\mathrm{T}}(\mathbf{H}-\mathbf{D}\mathbf{E})+\delta\mathbf{H}^{\mathrm{T}}(\mathbf{E}-\mathbf{e})-\delta\mathbf{e}^{\mathrm{T}}\mathbf{H} + \delta\mathbf{v}^{\mathrm{T}}\mathbf{P}]\bar{A}_1^{e\ell}\bar{A}_2^{e\ell}\mathrm{d}\xi_1\mathrm{d}\xi_2+\oint_{\Gamma^{e\ell}}\delta\mathbf{v}_\Gamma^{\mathrm{T}}\hat{\mathbf{H}}_\Gamma(1+k_N\bar{\delta})\mathrm{d}s=0, \tag{1}$$

$$\mathbf{v}=[v_1^-\ v_1^+\ v_2^-\ v_2^+\ v_3^-\ v_3^+]^{\mathrm{T}},\quad \mathbf{v}_\Gamma=[v_v^-\ v_v^+\ v_t^-\ v_t^+\ v_3^-\ v_3^+]^{\mathrm{T}},$$
$$\mathbf{e}=[e_{11}^-\ e_{11}^+\ e_{22}^-\ e_{22}^+\ 2e_{12}^-\ 2e_{12}^+\ 2e_{13}^-\ 2e_{13}^+\ 2e_{23}^-\ 2e_{23}^+\ e_{33}]^{\mathrm{T}},$$
$$\mathbf{E}=[E_{11}^-\ E_{11}^+\ E_{22}^-\ E_{22}^+\ 2E_{12}^-\ 2E_{12}^+\ 2E_{13}^-\ 2E_{13}^+\ 2E_{23}^-\ 2E_{23}^+\ E_{33}]^{\mathrm{T}},$$
$$\mathbf{H}=[H_{11}^-\ H_{11}^+\ H_{22}^-\ H_{22}^+\ H_{12}^-\ H_{12}^+\ H_{13}^-\ H_{13}^+\ H_{23}^-\ H_{23}^+\ H_{33}]^{\mathrm{T}},$$
$$\hat{\mathbf{H}}_\Gamma=[\hat{H}_{vv}^-\ \hat{H}_{vv}^+\ \hat{H}_{vt}^-\ \hat{H}_{vt}^+\ \hat{H}_{v3}^-\ \hat{H}_{v3}^+]^{\mathrm{T}},$$
$$\mathbf{P}=[-p_1^-\ p_1^+\ -p_2^-\ p_2^+\ -p_3^-\ p_3^+]^{\mathrm{T}},$$

where $\bar{A}_\gamma^{e\ell}=\bar{A}_\gamma\ell_\gamma^{e\ell}$ are the Lamé coefficients of the middle surface $\bar{S}^{e\ell}$ of the element; $\xi_\gamma=(\alpha_\gamma-d_\gamma^{e\ell})/l_\gamma^{e\ell}$ are the local

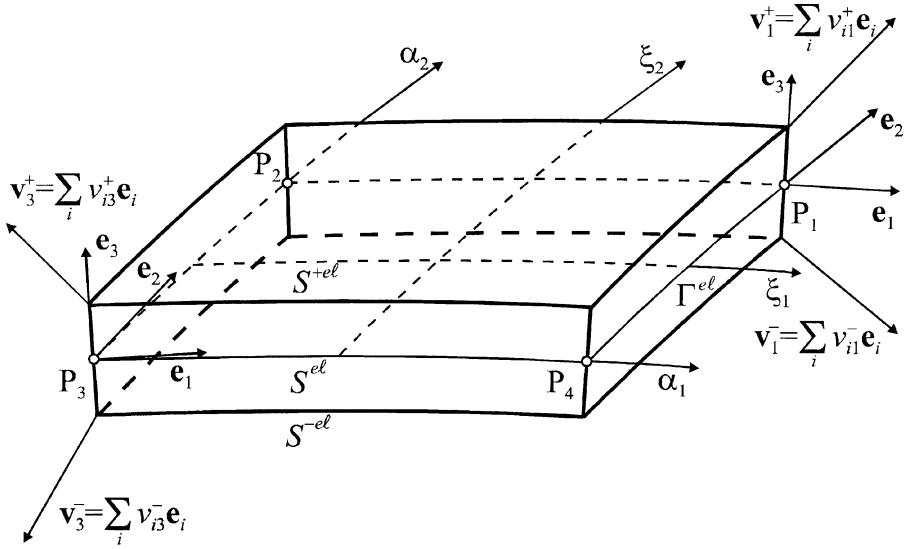

FIG. 1. Four-node ESL shell element.

curvilinear normalized coordinates (Figure 1); $d_\gamma^{e\ell} = (\alpha_\gamma^{-el} + \alpha_\gamma^{+el})/2$ are the coordinates of the center of the element; $2l_\gamma^{e\ell} = \alpha_\gamma^{+el} - \alpha_\gamma^{-el}$ are the lengths of the element, where $\gamma = 1$ and 2; $\mathbf{v}$ and $\mathbf{v}_\Gamma$ are the displacement vectors of the face surfaces in the $\alpha_1, \alpha_2, \alpha_3$ and v, t, α_3 coordinate systems, respectively; $\mathbf{e}$ is the displacement-dependent strain vector; $\mathbf{E}$ is the displacement-independent strain vector; $\mathbf{H}$ is the stress resultant vector; $\hat{\mathbf{H}}_\Gamma$ is the loading resultant vector acting on the edge of the element; $\mathbf{P}$ is the surface traction vector; $\mathbf{D}$ is the constitutive stiffness matrix of order 11×11, which components are defined in accordance with work [1].

For the simplest quadrilateral four-node shell element, the displacement field is approximated according to the standard C^0 interpolation

$$\mathbf{v} = \sum_r N_r \mathbf{v}_r, \quad \mathbf{v}_r = [v_{1r}^- \; v_{1r}^+ \; v_{2r}^- \; v_{2r}^+ \; v_{3r}^- \; v_{3r}^+]^{\mathrm{T}}, \tag{2}$$

where $\mathbf{v}_r$ are the displacement vectors of the element nodes; $N_r(\xi_1, \xi_2)$ are the linear shape functions of the element; and the index r runs from 1 to 4 and denotes a number of nodes. The load vector is also assumed to vary linearly inside the element.

In a result for displacement-dependent strains (3) from paper [1] we have the following approximation:

$$\mathbf{e} = \sum_{r_1,r_2} \xi_1^{r_1} \xi_2^{r_2} \mathbf{e}^{r_1 r_2}, \qquad \mathbf{e}^{r_1 r_2} = \mathbf{B}^{r_1 r_2} \mathbf{V}, \tag{3}$$

$$\mathbf{e}^{r_1 r_2} = \left[e_{11}^{-r_1 r_2} \; e_{11}^{+r_1 r_2} \; e_{22}^{-r_1 r_2} \; e_{22}^{+r_1 r_2} 2e_{12}^{-r_1 r_2} \; 2e_{12}^{+r_1 r_2} \; 2e_{13}^{-r_1 r_2} \; 2e_{13}^{+r_1 r_2} \; 2e_{23}^{-r_1 r_2} \; 2e_{23}^{+r_1 r_2} \; e_{33}^{r_1 r_2}\right]^{\mathrm{T}},$$

$$\mathbf{V} = \left[\mathbf{v}_1^{\mathrm{T}} \; \mathbf{v}_2^{\mathrm{T}} \; \mathbf{v}_3^{\mathrm{T}} \; \mathbf{v}_4^{\mathrm{T}}\right]^{\mathrm{T}},$$

where $\mathbf{V}$ is the displacement vector at nodal points of the element; $\mathbf{B}^{r_1 r_2}$ is the matrices of order 11×24 corresponding to the strain-displacement transformation. Throughout this section superscripts r_1, r_2 take the values 0 and 1.

To avoid shear and membrane locking and have no spurious zero energy modes, the assumed strain and stress resultant fields [5] inside the element are introduced

$$\mathbf{E} = \sum_{r_1,r_2} \xi_1^{r_1} \xi_2^{r_2} \mathbf{Q}^{r_1 r_2} \mathbf{E}^{r_1 r_2}, \tag{4}$$

$$\mathbf{E}^{00} = \left[E_{11}^{-00} \; E_{11}^{+00} \; E_{22}^{-00} \; E_{22}^{+00} \; 2E_{12}^{-00} \; 2E_{12}^{+00} \; 2E_{13}^{-00} \; 2E_{13}^{+00} \; 2E_{23}^{-00} \; 2E_{23}^{+00} \; E_{33}^{00}\right]^{\mathrm{T}},$$

$$\mathbf{E}^{01} = \left[E_{11}^{-01} \; E_{11}^{+01} \; 2E_{13}^{-01} \; 2E_{13}^{+01} \; E_{33}^{01}\right]^{\mathrm{T}},$$

$$\mathbf{E}^{10} = \left[E_{22}^{-10} \; E_{22}^{+10} \; 2E_{23}^{-10} \; 2E_{23}^{+10} \; E_{33}^{10}\right]^{\mathrm{T}}, \quad \mathbf{E}^{11} = \left[E_{33}^{11}\right],$$

$$\mathbf{H} = \sum_{r_1,r_2} \xi_1^{r_1} \xi_2^{r_2} \mathbf{Q}^{r_1 r_2} \mathbf{H}^{r_1 r_2}, \tag{5}$$

$$\mathbf{H}^{00} = \left[H_{11}^{-00} \; H_{11}^{+00} \; H_{22}^{-00} \; H_{22}^{+00} \; H_{12}^{-00} \; H_{12}^{+00} \; H_{13}^{-00} \; H_{13}^{+00} \; H_{23}^{-00} \; H_{23}^{+00} \; H_{33}^{00}\right]^{\mathrm{T}},$$

$$\mathbf{H}^{01} = \left[H_{11}^{-01} \; H_{11}^{+01} \; H_{13}^{-01} \; H_{13}^{+01} \; H_{33}^{01}\right]^{\mathrm{T}},$$

$$\mathbf{H}^{10} = \left[H_{22}^{-10} \; H_{22}^{+10} \; H_{23}^{-10} \; H_{23}^{+10} \; H_{33}^{10}\right]^{\mathrm{T}}, \quad \mathbf{H}^{11} = \left[H_{33}^{11}\right],$$

$$\mathbf{Q}^{01}=\begin{bmatrix}1&0&0&0&0\\0&1&0&0&0\\0&0&0&0&0\\0&0&0&0&0\\0&0&0&0&0\\0&0&0&0&0\\0&0&1&0&0\\0&0&0&1&0\\0&0&0&0&0\\0&0&0&0&0\\0&0&0&0&1\end{bmatrix},\quad \mathbf{Q}^{10}=\begin{bmatrix}0&0&0&0&0\\0&0&0&0&0\\1&0&0&0&0\\0&1&0&0&0\\0&0&0&0&0\\0&0&0&0&0\\0&0&0&0&0\\0&0&0&0&0\\0&0&1&0&0\\0&0&0&1&0\\0&0&0&0&1\end{bmatrix},\mathbf{Q}^{11}=\begin{bmatrix}0\\0\\0\\0\\0\\0\\0\\0\\0\\0\\1\end{bmatrix},$$

where $\mathbf{Q}^{00}$ is the identity matrix of order 11×11; $\mathbf{E}^{00}$ and $\mathbf{H}^{00}$ are the vectors of homogeneous states of strains and stress resultants; and $\mathbf{E}^{01}$, $\mathbf{E}^{10}$, $\mathbf{E}^{11}$ and $\mathbf{H}^{01}$, $\mathbf{H}^{10}$, $\mathbf{H}^{11}$ are the vectors of higher approximation modes of strains and stress resultants. Note that this approach may be treated as an assumed stress-strain formulation and was proposed by Wempner et al. [2] for the geometrically linear first-order shear deformation shell theory. Further developments for the Timoshenko beam, Mindlin plate, and Timoshenko-Mindlin-type shell theories with account for the thickness strain can be found in works [3–6]. Herein, the more general study based on the ESL shell theory is presented.

Substituting approximations (2)–(5) into the mixed variational Eq. (1) and using a standard variational procedure, one derives governing equations of the developed finite element formulation

$$\mathbf{E}^{r_1r_2}=(\mathbf{Q}^{r_1r_2})^{\mathrm{T}}\,\mathbf{B}^{r_1r_2}\mathbf{V}, \tag{6a}$$

$$\mathbf{H}^{r_1r_2}=(\mathbf{Q}^{r_1r_2})^{\mathrm{T}}\,\mathbf{D}\mathbf{Q}^{r_1r_2}\mathbf{E}^{r_1r_2}, \tag{6b}$$

$$\sum_{r_1,r_2}\frac{1}{3^{r_1+r_2}}(\mathbf{B}^{r_1r_2})^{\mathrm{T}}\,\mathbf{Q}^{r_1r_2}\,\mathbf{H}^{r_1r_2}=\mathbf{F}, \tag{6c}$$

where $\mathbf{F}$ is the force vector.

Eliminating further strains and stress resultants from Eq. (6), we arrive at the element equilibrium equations

$$\mathbf{K}\mathbf{V}=\mathbf{F}, \tag{7}$$

where $\mathbf{K}$ is the elemental stiffness matrix defined as

$$\mathbf{K}=\sum_{r_1,r_2}\frac{1}{3^{r_1+r_2}}(\mathbf{B}^{r_1r_2})^{\mathrm{T}}\mathbf{Q}^{r_1r_2}(\mathbf{Q}^{r_1r_2})^{\mathrm{T}}\mathbf{D}\mathbf{Q}^{r_1r_2}(\mathbf{Q}^{r_1r_2})^{\mathrm{T}}\mathbf{B}^{r_1r_2}. \tag{8}$$

Proposition *The transverse shear and normal displacement-independent strains satisfy the following coupling conditions*:

$$hE_{33}^{10}=2A_1^{e\ell}\big(E_{13}^{+00}-E_{13}^{-00}\big),\quad hE_{33}^{11}=2A_1^{e\ell}\big(E_{13}^{+01}-E_{13}^{-01}\big), \tag{9a}$$

$$hE_{33}^{01}=2A_2^{e\ell}\big(E_{23}^{+00}-E_{23}^{-00}\big),\quad hE_{33}^{11}=2A_2^{e\ell}\big(E_{23}^{+10}-E_{23}^{-10}\big), \tag{9b}$$

Proof. Substituting Eq. (3) into linking conditions for the displacement-dependent strains (4) yields (see Proposition 1 in work [1])

$$2A_1^{e\ell}\big(e_{13}^{+00}-e_{13}^{-00}\big)=he_{33}^{10},\quad 2A_1^{e\ell}\big(e_{13}^{+01}-e_{13}^{-01}\big)=he_{33}^{11}, \tag{10a}$$

$$2A_2^{e\ell}\big(e_{23}^{+00}-e_{23}^{-00}\big)=he_{33}^{01},\quad 2A_2^{e\ell}\big(e_{23}^{+10}-e_{23}^{-10}\big)=he_{33}^{11}, \tag{10b}$$

From Eq. (6a) with account for Eqs. (3) and (10a) the first group of required relations (9a) are obtained

$$2A_1^{e\ell}\big(E_{13}^{+00}-E_{13}^{-00}\big)=2A_1^{e\ell}\big(e_{13}^{+00}-e_{13}^{-00}\big)=he_{33}^{10}=hE_{33}^{10},$$
$$2A_1^{e\ell}\big(E_{13}^{+01}-E_{13}^{-01}\big)=2A_1^{e\ell}\big(e_{13}^{+01}-e_{13}^{-01}\big)=he_{33}^{11}=hE_{33}^{11}.$$

The remaining relations (9b) can be deduced by using Eqs. (3), (6a) and (10b). ■

Coupling equations (9) play a central role in our finite element formulation because they imply that only 18 assumed strain modes are *independent* of 22 modes from approximation (4). In a result, all constructed elemental stiffness matrices have six, and only six, zero eigenvalues as required for satisfaction of the general rigid-body motion representation, since 24 displacement degrees of freedom are introduced. It should be mentioned that our elemental stiffness matrices require only direct substitutions, that is, no inversion is needed if sides of the element coincide with lines of principal curvatures of the reference surface. Furthermore, they are evaluated by using the analytical integration. Therefore, our finite element formulation is very economical and efficient compared to the conventional isoparametric finite element formulations because it reduces the costly numerical integration by deriving the elemental stiffness matrices.

In order to carry out the analytical integration in the 2D integral from Eq. (1), displacement-dependent strains (3) with account for relationships (9) and (10) from work [1] are evaluated by using the following schemes:

$$e_{\alpha\alpha}^{\pm r_1r_2}=\{\zeta_\alpha^{\pm}\}^{00}\lambda_\alpha^{\pm r_1r_2},\ 2e_{12}^{\pm r_1r_2}=\{\zeta_2^{\pm}\}^{00}\omega_1^{\pm r_1r_2}+\{\zeta_1^{\pm}\}^{00}\omega_2^{\pm r_1r_2}, \tag{11a}$$

$$2e_{\alpha3}^{\pm r_1r_2}=\{\zeta_\alpha^{\pm}\}^{00}\beta_\alpha^{r_1r_2}-\theta_\alpha^{\pm r_1r_2},\quad e_{33}^{r_1r_2}=\beta_3^{r_1r_2}, \tag{11b}$$

where

$$\lambda_\alpha^{\pm r_1r_2}=\left\{\frac{1}{A_\alpha^{e\ell}}v_\alpha^{\pm}\right\}_\alpha^{r_1r_2}+\left\{B_{\alpha\alpha}^{e\ell}v_\alpha^{\pm}+B_{\alpha\beta}^{e\ell}v_\beta^{\pm}+k_\alpha v_3^{\pm}\right\}^{r_1r_2}\quad(\beta\neq\alpha), \tag{12}$$

$$\omega_\alpha^{\pm r_1r_2}=\left\{\frac{1}{A_\alpha^{e\ell}}v_\beta^{\pm}\right\}_\alpha^{r_1r_2}+\left\{B_{\alpha\alpha}^{e\ell}v_\beta^{\pm}-B_{\alpha\beta}^{e\ell}v_\alpha^{\pm}\right\}^{r_1r_2}\quad(\beta\neq\alpha),$$

$$\theta_{\alpha}^{\pm r_1 r_2} = -\left\{\frac{1}{A_{\alpha}^{e\ell}} v_3^{\pm}\right\}_{\alpha}^{r_1 r_2} + \left\{-B_{\alpha\alpha}^{e\ell} v_3^{\pm} + k_{\alpha} v_{\alpha}^{\pm}\right\}^{r_1 r_2},$$
$$\beta_i^{r_1 r_2} = \frac{1}{h}\{v_i^{\pm} - v_i^{-}\}^{r_1 r_2}.$$

In formulas (11) and (12) in accordance with Figure 1 convenient mesh notations are employed

$$\{f\}^{00} = \frac{1}{4}[f(P_1) + f(P_2) + f(P_3) + f(P_4)],$$
$$\{f\}^{01} = \frac{1}{4}[f(P_1) + f(P_2) - f(P_3) - f(P_4)], \qquad (13)$$
$$\{f\}^{10} = \frac{1}{4}[f(P_1) - f(P_2) - f(P_3) + f(P_4)],$$
$$\{f\}^{11} = \frac{1}{4}[f(P_1) - f(P_2) + f(P_3) - f(P4)],$$
$$\{f\}_1^{00} = \{f\}^{10}, \quad \{f\}_1^{01} = \{f\}^{11}, \quad \{f\}_1^{10} = \{f\}_1^{11} = 0,$$
$$\{f\}_2^{00} = \{f\}^{01}, \quad \{f\}_2^{10} = \{f\}^{11}, \quad \{f\}_2^{01} = \{f\}_2^{11} = 0.$$

In regards to a product $\bar{A}_1^{e\ell}\bar{A}_2^{e\ell}$ from variational Eq. (1), it does not vary inside the element. Allowing for notations (13) the simplest approximation is used

$$\bar{A}_1^{e\ell}\bar{A}_2^{e\ell} = \left\{\bar{A}_1^{e\ell}\bar{A}_2^{e\ell}\right\}^{00}.$$

§3. NUMERICAL TESTS

The performance of the proposed four-node ESL shell elements is evaluated with several problems extracted from the literature. A listing of these elements and the abbreviations used to identify them are contained in Table 1. It should be mentioned, in advance, that ESLSr4 and ESLSs4 elements are slightly distinguishable for engineering calculations.

3.1. Isotropic Plate under Sinusoidal Loading

A simply supported rectangular isotropic plate depicted in Figure 2 is subjected to the sinusoidally distributed pressure load

$$p_3^{+} = p_0 \sin\frac{\pi\alpha_1}{a}\sin\frac{\pi\alpha_2}{b}, \quad p_3^{-} = 0,$$

where a and b are two in-plane dimensions of the plate.

We will search an exact solution of the problem in a form

$$v_1^{\pm} = v_{10}^{\pm}\cos\frac{\pi\alpha_1}{a}\sin\frac{\pi\alpha_2}{b}, \quad v_2^{\pm} = v_{20}^{\pm}\sin\frac{\pi\alpha_1}{a}\cos\frac{\pi\alpha_2}{b},$$
$$v_3^{\pm} = v_{30}^{\pm}\sin\frac{\pi\alpha_1}{a}\sin\frac{\pi\alpha_2}{b}, \qquad (14)$$
$$u_{i0} = \bar{v}_{i0} + \alpha_3\beta_{i0}, \quad \bar{v}_{i0} = \frac{1}{2}(v_{i0}^{-} + v_{i0}^{+}), \quad \beta_{i0} = \frac{1}{2}(v_{i0}^{+} - v_{i0}^{-}), \qquad (15)$$

TABLE 1
Listing of developed shell formulations

Name	Description
ESLSc ESLSc4	ESL shell formulation and a corresponding four-node curved shell element based on the complete constitutive law [1] (Section 4.1)
ESLSm ESLSm4	ESL shell formulation and a corresponding four-node curved shell element based on the modified constitutive law [1] (Section 4.2)
ESLSr ESLSr4	ESL shell formulation and a corresponding four-node curved shell element based on the reduced constitutive law [1] (Section 4.3)
ESLSs ESLSs4	ESL shell formulation and a corresponding four-node curved shell element based on the simplified constitutive law [1] (Section 4.4)
LWSr	LW shell formulation based on the reduced constitutive law [1] (Section 4.3)
LWSr$^{\mathrm{I}}$	LW shell formulation based on the reduced constitutive law [1] (Section 4.3) with I equally located fictitious interfaces inside each layer (I = 1 and 3)

where $\bar{v}_{io} = u_{i0}(0)$ are the displacements in a center of the middle plane. Omitting trivial calculations one can obtain the following solutions for all four ESL plate theories:

- ESLSc solution

$$\bar{v}_{30} = hV_3\left[\frac{1-2\nu}{(1-\nu)^2} + \frac{\Theta}{1-\nu}\right],$$
$$\beta_{30} = -\frac{p_0}{E}\left[\frac{2}{1-\nu^2} + \frac{\Theta}{2(1+\nu)}\right]^{-1}; \qquad (16a)$$

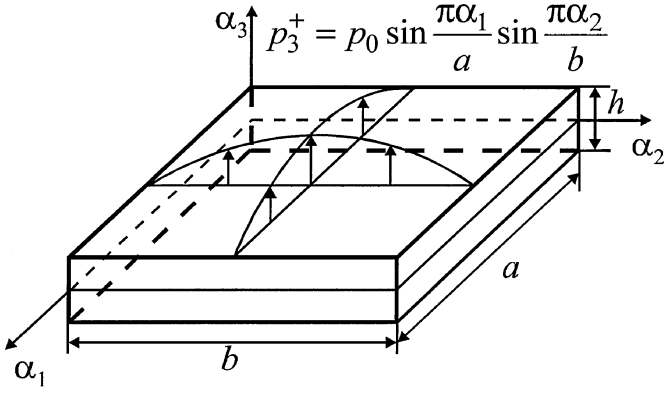

$$a = b = 3,\ E = 10^7,\ \nu = 0.3$$

FIG. 2. Rectangular plate under sinusoidal loading.

- ESLSm solution

$$\bar{v}_{30} = hV_3\left(1+\frac{\Theta}{1-\nu}\right),$$
$$\beta_{30} = -\frac{p_0}{E}\left[\frac{2}{1-\nu^2}+\frac{\Theta}{2(1+\nu)}\right]^{-1}; \qquad (16b)$$

- ESLSr and ESLSs solutions

$$\bar{v}_{30} = hV_3\left(1+\frac{\Theta}{1-\nu}\right),$$
$$\beta_{30} = -\frac{p_0}{E}\left[2+\frac{\Theta}{2(1+\nu)}\right]^{-1}, \qquad (16c)$$

where V_3 is the dimensionless transverse displacement in a center of the plate for the classical plate theory (CPT) defined as

$$V_3 = \frac{12(1-\nu^2)(a/h)^4 p_0}{\pi^4(1+a^2/b^2)^2 E}, \quad \Theta = \frac{\pi^2(1+a^2/b^2)}{6(a/h)^2}.$$

Comparing corresponding expressions in formulas (16a)–(16c) one can observe that due to difference of the first terms thickness locking occurs. However, for the zero Poisson's ratio all four theories lead to identical solutions.

Table 2 displays the dimensionless transverse displacement

$$U_3 = \frac{100Eh^3}{p_0 a^4}u_{30}$$

in a center of the square plate ($a = b$) for various values of the transverse coordinate α_3. A comparison with analytical solutions on the basis of the elasticity theory [9] and CPT [10] is also given. It is seen that the ESL plate theory based on the complete 3D constitutive law demonstrates significant thickness locking.

TABLE 2
Distribution of dimensionless transverse displacement U_3 in thickness direction of square isotropic plate. Analytical solutions

$\frac{a}{h}$	$\frac{\alpha_3}{h}$	Elasticity theory [9]	ESLSc	ESLSm	ESLSr	ESLSs	CPT [10]
3	−0.5	3.882	3.487	4.002	3.978	3.978	2.803
	0.0	4.309	3.751	4.266	4.266	4.266	2.803
	0.5	4.440	4.015	4.530	4.555	4.555	2.803
10	−0.5	2.912	2.417	2.932	2.932	2.932	2.803
	0.0	2.942	2.420	2.934	2.934	2.934	2.803
	0.5	2.917	2.422	2.937	2.937	2.937	2.803
10^3	0.0	2.803	2.288	2.803	2.803	2.803	2.803

TABLE 3
Distribution of dimensionless transverse displacement U_3 in thickness direction of square isotropic plate. Finite element solutions

		ESLSc4 element		ESLSm4 element		ESLSr4 element	
$\frac{a}{h}$	$\frac{\alpha_3}{h}$	8 × 8	32 × 32	8 × 8	32 × 32	8 × 8	32 × 32
3	−0.5	3.465	3.486	3.975	4.000	3.951	3.976
	0.0	3.728	3.750	4.239	4.264	4.239	4.264
	0.5	3.992	4.014	4.502	4.528	4.527	4.553
10^3	0.0	2.270	2.287	2.780	2.801	2.780	2.801

Table 3 lists the results of the numerical study. Due to symmetry of the problem only one quarter of the plate is discretized by using regular meshes of the ESLS4 elements. As can be seen, corresponding results from Tables 2 and 3 agree closely. So, our finite element formulations based on the modified and reduced stress-strain relationships are completely free from shear and thickness locking phenomena. Note also that predictions of the ESLSr4 and ESLSs4 elements are exactly the same and, therefore, the ESLSs4 element solution is not listed in Table 3.

3.2. Cylindrical Bending of Cross-Ply Plate under Sinusoidal Loading

The simply supported cross-ply plate in cylindrical bending (see Figure 3) is subjected to the sinusoidally distributed pressure load. Here, subscripts L and T refer to the fiber and transverse directions of the individual ply, and the fiber direction coincides

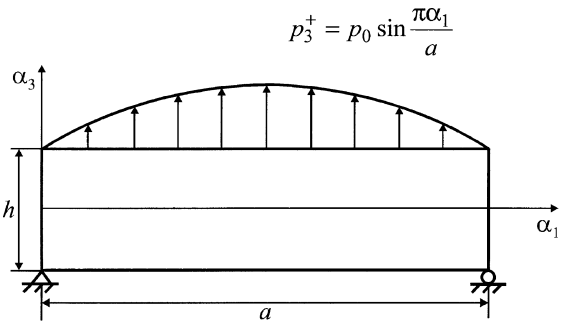

$$a = 1,\ h_J = h/J\ \ (J = 2,3 \text{ and } 4),$$
$$E_L = 2.5\times10^7,\ E_T = 10^6,\ G_{LT} = 5\times10^5,\ G_{TT} = 2\times10^5,$$
$$\nu_{LT} = \nu_{TT} = 0.25$$

(A) Ply thickness $= [h_3/h_3/h_3]$, Ply orientation $= [0/90/0]$
(B) Ply thickness $= [h_4/h_4/h_4/h_4]$, Ply orientation $= [90/0/90/0]$
(C) Ply thickness $= [h_4/h_2/h_4]$, Ply orientation $= [30/-30/30]$
(D) Ply thickness $= [h_4/h_2/h_4]$, Ply orientation $= [60/-60/60]$

FIG. 3. Cylindrical bending of laminated composite plate under sinusoidal loading.

TABLE 4
Dimensionless transverse displacement $100E_T h^3 \bar{v}_{30}/p_0 a^4$ at center point of laminated composite plate in cylindrical bending

	Problem A		Problem B		Problem C	
	$a/h = 4$	$a/h = 6$	$a/h = 4$	$a/h = 6$	$a/h = 4$	$a/h = 6$
Elasticity [11]	2.887	1.635	4.181	2.556		
LWPM1 [12]*	2.904	1.634	3.300	2.095		
LWPM1 [13]	2.907	1.636	3.316	2.107		
LWPM1 [14, 15]	2.907	1.636	4.202	2.561	3.318	2.019
LWPM3 [12]	2.881	1.634	4.102	2.514		
Present formulations						
LWSr	2.790	1.587	4.067	2.505	3.227	1.980
LWSr[1]	2.848	1.621	4.148	2.548	3.258	2.001
LWSr[3]	2.882	1.634	4.178	2.561	3.296	2.014
ESLSm4	2.090	1.211	2.924	1.922	2.569	1.631
ESLSr4	2.092	1.213	2.924	1.926	2.576	1.637
ESLSs4	2.092	1.213	2.924	1.926	2.576	1.637

*LWPM1 and LWPM3 denote plate models based on the Hellinger-Reissner mixed variational principle with linear and cubic displacement fields.

with α_1 coordinate direction in the top layer for both investigated problems A and B.

Due to symmetry of the problem, one half of the plate is discretized by using a 32×1 mesh of ESLS4 elements. Table 4 lists the dimensionless transverse displacement at the center point of the plate for various values of the slenderness ratio a/h. Additionally, a comparison with analytical solutions of the elasticity theory [11], present LW shell theory, and extracted from the literature LW plate formulations [12–15], based on the Hellinger-Reissner variational principle, are also given. One can observe that predictions of all ESLS4 elements are close and they yield, as expected, the decreased values of the transverse displacement for thick laminated composite plates, while the LWSr model performs well, especially its version with fictitious interfaces inside layers.

Figures 4 and 5 show the distribution of dimensionless transverse stresses in the thickness direction. The transverse components of the stress tensor are computed by integrating the 3D elasticity equations with account for equilibrium conditions at the layer interfaces and boundary conditions on the bottom surface [16, 17]. Due to this approach, the boundary conditions for the transverse components on the top surface are also *satisfied*. It is seen that all results agree closely, especially Pagano's and LWSr solutions.

3.3. Cylindrical Bending of Angle-Ply Plate under Sinusoidal Loading

Consider a problem of cylindrical bending for the simply supported three-layer angle-ply plate subjected to the sinusoidally distributed pressure load. This problem has been chosen for numerical testing in the anisotropic plate response [18], since all components of the displacement vector are different from zero but independent on α_2 coordinate. The geometrical and material data of the angle-ply plate are given in Figure 3, where an angle between the fiber direction and α_1-axis is measured in the clockwise direction and equal to 30° and 60° for problems C and D, respectively.

Figure 6 and Table 4 present the dimensionless transverse displacement at the center point of the plate for various values of the slenderness ratio, and a comparison with the elasticity

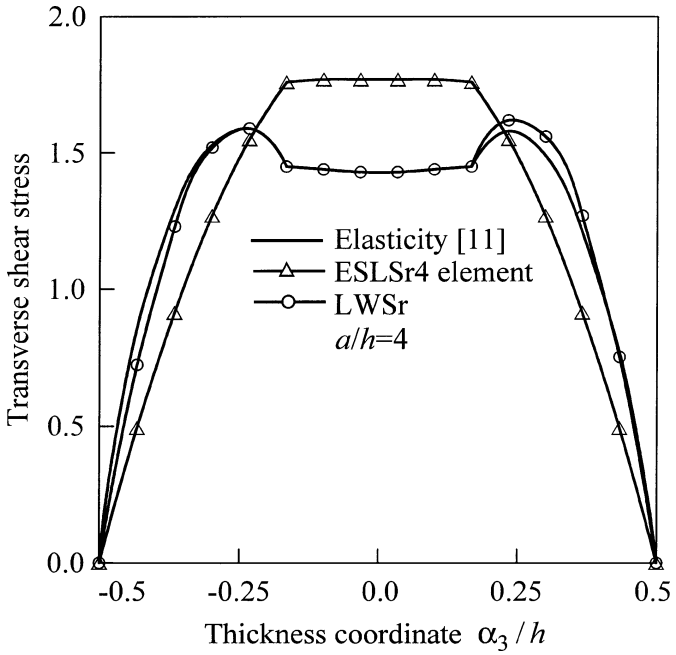

FIG. 4. Distribution of transverse shear stress σ_{13}/p_0 in thickness direction at $\alpha_1 = 0$ of three-layer cross-ply plate (Problem A).

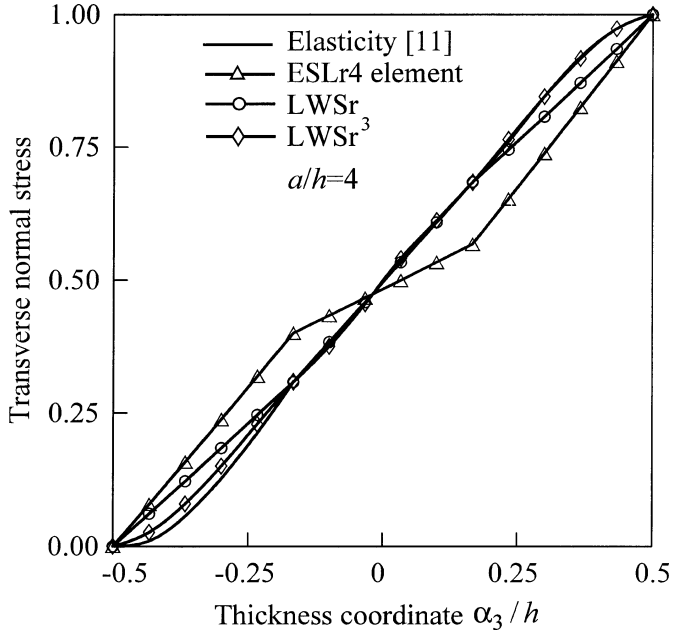

FIG. 5. Distribution of transverse normal stress σ_{33}/p_0 in thickness direction at $\alpha_1 = a/2$ of three-layer cross-ply plate (Problem A).

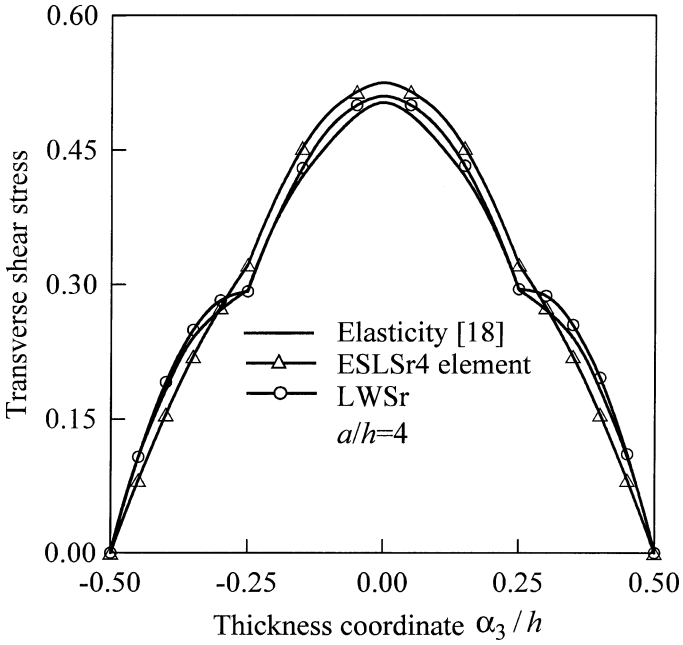

FIG. 7. Distribution of transverse shear stress $\sigma_{13}h/p_0a$ in thickness direction at $\alpha_1 = 0$ of three-layer angle-ply plate (Problem C).

theory [18]. One may see that each curve, corresponding to problems C and D, asymptotically approaches the CPT solution that is displayed by the horizontal line through unity. It should be mentioned that both coordinates in Figure 6 are plotted on *log* scales [18]. Figure 7 and 8 demonstrate the distribution of transverse shear stresses in the thickness direction. An algorithm described in the previous section has been applied. Additionally, Table 5 lists results obtained by using the LWSr formulation and LWSr^3 one as well. A case of changing the loading plane is also presented.

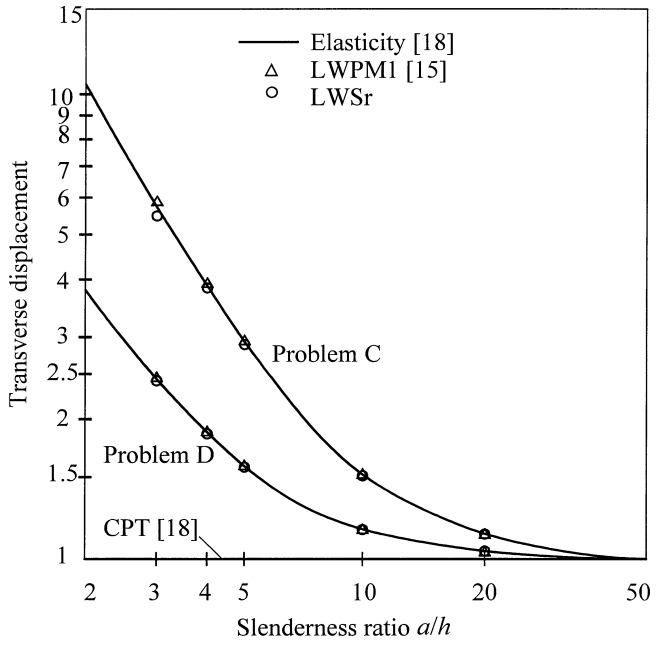

FIG. 6. Dimensionless transverse displacement $Q_{11}\pi^4 h^3 \bar{v}_{30}/12 p_0 a^4$ at center point of three-layer angle-ply plate for Problem C ($Q_{11} = 1.4629 \times 10^7$) and problem D ($Q_{11} = 2.5993 \times 10^6$).

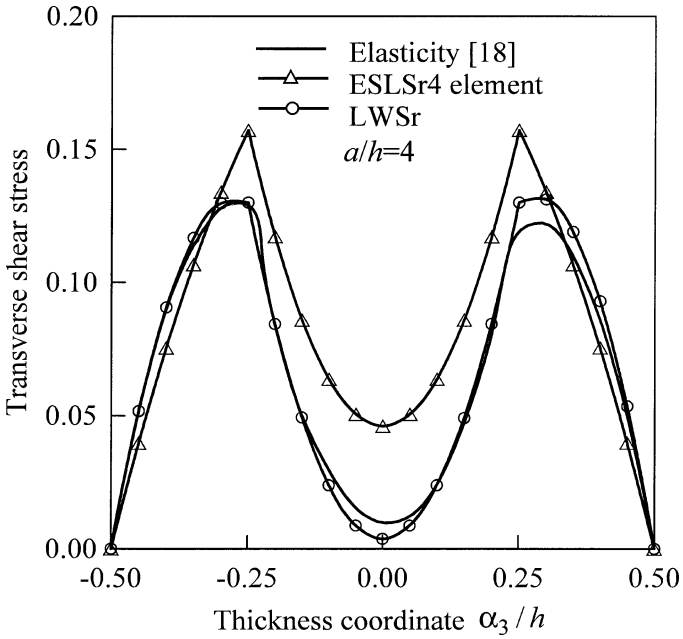

FIG. 8. Distribution of transverse shear stress $\sigma_{23}h/p_0a$ in thickness direction at $\alpha_1 = a$ of three-layer angle-ply plate (Problem C).

TABLE 5
Distribution of transverse stresses in thickness direction of three-layer angle-ply plate (Problem C)

	Thickness coordinate α_3/h						
	−0.5	−0.375	−0.25	0.0	0.25	0.375	0.5
LWSr for $p_3^- = 0$ and $p_3^+ = p_0 \sin(\pi\alpha_1/a)$							
$\sigma_{13}(0, \alpha_3)/p_0$	0.00	0.89	1.17	2.04	1.18	0.92	0.00
$10\sigma_{23}(a, \alpha_3)/p_0$	0.00	4.22	5.20	0.15	5.20	4.31	0.00
$10\sigma_{33}(a/2, \alpha_3)/p_0$	0.00	0.77	1.55	4.94	8.42	9.19	10.0
LWSr^3 for $p_3^- = 0$ and $p_3^+ = p_0 \sin(\pi\alpha_1/a)$							
$\sigma_{13}(0, \alpha_3)/p_0$	0.00	0.90	1.17	2.01	1.18	0.92	0.00
$10\sigma_{23}(a, \alpha_3)/p_0$	0.00	4.23	5.19	0.32	5.19	4.33	0.00
$10\sigma_{33}(a/2, \alpha_3)/p_0$	0.00	0.50	1.56	4.98	8.41	9.48	10.0
LWSr for $p_3^- = p_0 \sin(\pi\alpha_1/a)$ and $p_3^+ = 0$							
$\sigma_{13}(0, \alpha_3)/p_0$	0.00	0.92	1.18	2.04	1.17	0.89	0.00
$10\sigma_{23}(a, \alpha_3)/p_0$	0.00	4.31	5.20	0.15	5.20	4.22	0.00
$10\sigma_{33}(a/2, \alpha_3)/p_0$	10.0	9.19	8.42	4.94	1.55	0.77	0.00

3.4. Pinched Cylindrical Shell with Rigid Diaphragms

To illustrate the capability of developed ESLS4 elements to overcome membrane and shear locking phenomena and to compare them with high performance four-node isoparametric elements [19–22], we consider one of the most demanding standard linear tests. A short cylindrical shell supported by two rigid diaphragms at the ends is loaded by two opposite concentrated forces in its middle section. The geometrical and material properties of the shell are shown in Figure 9.

Owing to symmetry of the problem, only one octant of the shell is modeled with regular meshes of ESLS4 elements. Table 6 displays the normalized transverse displacement under the applied load, and a comparison with above four-node quadrilateral elements. The displacements are normalized with respect to the analytical solution -1.8248×10^{-5} [23]. As can be seen, our results exhibit an excellent agreement even for coarse meshes although the ESLSc4 element is too stiff.

3.5. Pinched Three-Layer Cross-Ply Hyperbolic Shell

A cross-ply hyperbolic shell under two pairs of opposite concentrated forces (Figure 10) was considered by Basar et al. [24] for testing finite deformation formulations for composite shells, while we employ this example as a linear benchmark test to assess the proposed schemes (11)–(13) of the analytical integration. Besides, as in the pinched cylinder example, we can verify a proper representation of inextensional bending and, additionally, this is an excellent test for the ability of the element to model rigid-body motions. The geometrical parameters of the shell are expressed by

$$A_1 = \sqrt{1 + \frac{\mu^2 z^2}{A_2^2}}, \quad A_2 = r\sqrt{1 + \frac{\mu z^2}{r^2}}, \quad k_1 = -\frac{\mu r^2}{A_1^3 A_2^3},$$
$$k_2 = \frac{1}{A_1 A_2}, \quad \mu = \frac{R^2 - r^2}{L^2},$$

where $\alpha_1 = z \in [0, L]$, and $\alpha_2 \in [0, \pi/2]$ are the meridional and circumferential coordinates of the middle surface. The fiber

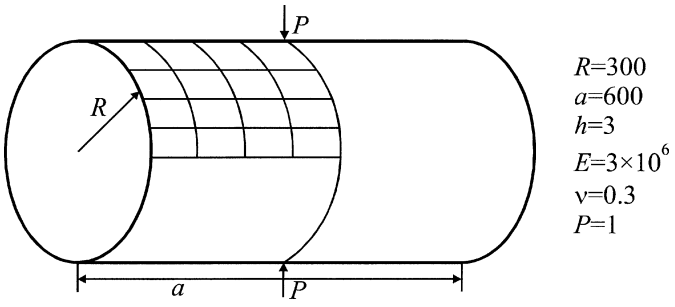

FIG. 9. Pinched cylindrical shell with rigid diaphragms.

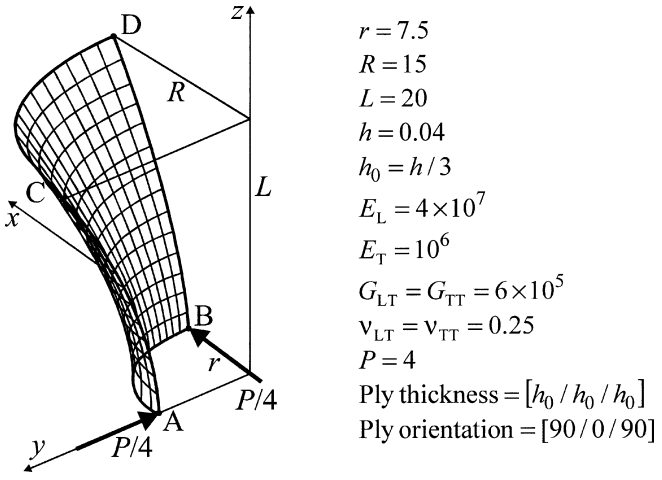

FIG. 10. Pinched three-layer cross-ply hyperbolic shell.

TABLE 6
Normalized transverse displacement $(\bar{v}_3)^{\text{Norm}}$ under applied load of pinched cylindrical shell with rigid diaphragms

	Isoparametric four-node elements				ESLS4 elements			
Mesh	[19]	[20]	[21]	[22]	ESLSc4	ESLSm4	ESLSr4	ESLSs4
4×4	0.373	0.469	0.370	0.399	0.7945	0.8881	0.8902	0.8900
8×8	0.747	0.791	0.740	0.763	0.8341	0.9406	0.9414	0.9412
16×16	0.935	0.946	0.930	0.935	0.8711	0.9862	0.9863	0.9861

direction coincides with α_2 coordinate direction in the outer layers.

Due to symmetry, only one octant of the shell is discretized with uniform meshes of ESLS4 elements. Table 7 lists normalized displacements at points A and C. The displacements are normalized with respect to values $-\bar{v}_y^{\text{A}} = \bar{v}_x^{\text{B}} = 0.1013$ and $\bar{v}_y^{\text{C}} = -\bar{v}_x^{\text{D}} = 0.09785$, respectively, where $\bar{v}_x$ and $\bar{v}_y$ denote displacements of the middle surface in x and y directions. Such values are the computationally exact solutions of this problem, based on the ESLSs formulation, taking into account the simplified constitutive law and consistent mesh refinements. One can observe that all developed elements perform well, but the ESLSs4 element is less expensive because of the simplicity of its constitutive stiffness matrix.

3.6. Thick-Walled Cylinder

In order to investigate a volumetric locking phenomenon, we consider the infinite thick-walled cylinder. The geometrical and material data of the problem are presented in Figure 11. The analytical solutions of the plane stress and the strain problems for the cylinder can be written in the following form [25, 26]:

$$u_1 = \frac{(1+\nu)r^2 p}{(R^2 - r^2)E}\left(\frac{R^2}{\rho} + \frac{1-\nu}{1+\nu}\rho\right) \text{ and}$$
$$u_1 = \frac{(1+\nu)r^2 p}{(R^2 - r^2)E}\left(\frac{R^2}{\rho} + (1-2\nu)\rho\right). \qquad (17)$$

Table 8 lists results derived by using the relatively large uniform 100×1 mesh of axisymmetric ESLS4 elements for the ring

TABLE 8
Radial displacement at inner surface of infinite thick-walled cylinder

Poisson's ratio	Plane stress problem	Plane strain problem	ESLS4 elements			
			ESLSc4	ESLSm4	ESLSr4	ESLSs4
0.0	3.750	3.750	3.749	3.749	3.749	3.749
0.3	4.650	4.583	4.582	4.582	4.649	4.649
0.49	5.220	5.040	5.035	5.035	5.219	5.219
0.499	5.247	5.060	5.013	5.013	5.246	5.246
0.5	5.250	5.063	—	—	5.249	5.249

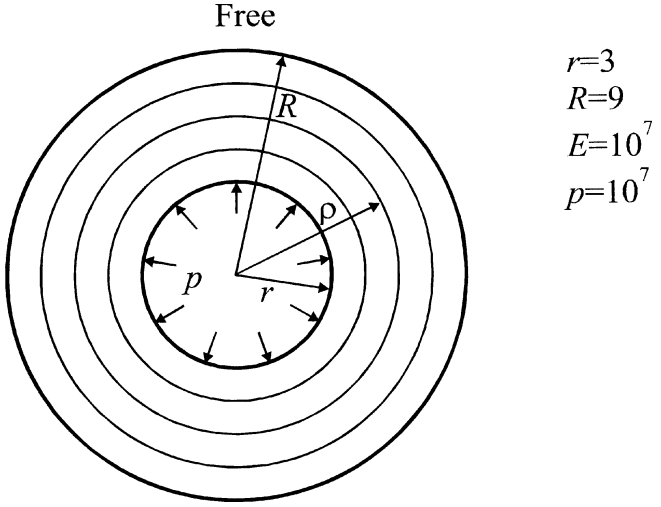

FIG. 11. Infinite thick-walled cylinder.

TABLE 7
Normalized displacements at points A and C of pinched cross-ply hyperbolic shell

	ESLSc4		ESLSm4		ESLSr4		ESLSs4	
Mesh	$(\bar{v}_y^A)^{\text{Norm}}$	$(\bar{v}_y^C)^{\text{Norm}}$	$(\bar{v}_y^A)^{\text{Norm}}$	$(\bar{v}_y^C)^{\text{Norm}}$	$(\bar{v}_y^A)^{\text{Norm}}$	$(\bar{v}_y^C)^{\text{Norm}}$	$(\bar{v}_y^A)^{\text{Norm}}$	$(\bar{v}_y^C)^{\text{Norm}}$
2×2	0.5941	1.1433	0.5941	1.1436	0.5961	1.1474	0.5961	1.1474
4×4	0.8692	1.0295	0.8694	1.0299	0.8726	1.0337	0.8726	1.0337
8×8	0.9572	1.0047	0.9575	1.0052	0.9610	1.0089	0.9610	1.0089
16×16	0.9839	0.9979	0.9842	0.9983	0.9881	1.0020	0.9879	1.0021

plate subjected to inner pressure to describe a geometrically linear plate response more precisely. The thickness of a plate is set to be $h = 1$. This problem is examined for a case of constraining all transverse displacement degrees of freedom to be zero as a boundary condition at the face planes. A comparison with exact solutions (17) is also given. It is seen that both ESLSr4 and ESLSs4 elements overcome volumetric locking excellently, and listed results correspond to the plane stress problem. As concerns ESLSc4 and ESLSm4 element solutions, they describe nearly incompressible materials well and converge, on the contrary, to the plane strain solution, but fail in the incompressibility limit.

§4. CONCLUSIONS

The simple and efficient assumed stress-strain four-node curved ESL shell elements have been formulated. The finite element formulation is based on the original approach in which displacement vectors of the bottom and top surfaces are introduced and resolved as in classical shell formulations in the local reference surface frame. So, as fundamental unknowns, six displacements of the face surfaces and, additionally, 11 strains and 11 conjugate stress resultants have been chosen. This allows, in particular, special loading conditions at the bottom and top surfaces and shell edges to be accounted for.

All four ESLS4 elements developed do not contain any spurious zero energy modes and possess six zero eigenvalues, but the ESLSc4 element is too stiff. It is noteworthy that all constructed elemental stiffness matrices require only direct substitutions (no inversion is needed) and they are evaluated by using the 3D analytical integration. Therefore, our finite element formulation is very simple and economical compared to conventional isoparametric formulations. But, for the thick-walled laminated composite structures, the developed ESL shell formulation cannot provide reliable results. For such a case, the LW shell formulation should be employed.

REFERENCES

1. G. M. Kulikov and S. V. Plotnikova, Equivalent Single-Layer and Layerwise Shell Theories and Rigid-Body Motions—Part I: Foundations, *Mech. Advanced Mater. Struct.*, vol. 12, 2005.
2. G. Wempner, D. Talaslidis, and C. M. Hwang, A Simple and Efficient Approximation of Shells via Finite Quadrilateral Elements, *J. Appl. Mech.*, vol. 49, pp. 115–120, 1982.
3. G. M. Kulikov and S. V. Plotnikova, Non-Conventional Non-Linear Two-Node Hybrid Stress-Strain Curved Beam Elements, *Finite Elements Anal. Des.*, vol. 40, pp. 1333–1359, 2004.
4. G. M. Kulikov and S. V. Plotnikova, Finite Deformation Plate Theory and Large Rigid-Body Motions, *Int. J. Non-Linear Mech.*, vol. 39, pp. 1093–1109, 2004.
5. G. M. Kulikov and S. V. Plotnikova, Simple and Effective Elements Based upon Timoshenko- Mindlin Shell Theory, *Comput. Meth. Appl. Mech. Eng.*, vol. 191, pp. 1173–1187, 2002.
6. G. M. Kulikov and S. V. Plotnikova, Non-Linear Strain-Displacement Equations Exactly Representing Large Rigid-Body Motions. Part I. Timoshenko-Mindlin Shell Theory, *Comput. Meth. Appl. Mech. Eng.*, vol. 192, pp. 851–875, 2003.
7. S. Ahmad, B. M. Irons, and O. C. Zienkiewicz, Analysis of Thick and Thin Shell Structures by Curved Shell Elements, *Int. J. Numer. Meth. Eng.*, vol. 2, pp. 419–451, 1970.
8. K. J. Bathe, *Finite Element Procedures*, Prentice Hall, New Jersey, 1996.
9. B. F. Vlasov, On the Bending of Rectangular Thick Plate, *Trans. Moscow State Univ.*, vol. 2, pp. 25–31, 1957 (in Russian).
10. S. P. Timoshenko and S. Woinowsky-Krieger, *Theory of Plates and Shells*, 2nd ed., McGraw-Hill, New York, 1959.
11. N. J. Pagano, Exact Solutions for Composite Laminates in Cylindrical Bending, *J. Composite Mater.*, vol. 3, pp. 398-411, 1969.
12. E. Carrera, Transverse Normal Stress Effects in Multilayered Plates, *J. Appl. Mech.*, vol. 66, pp. 1004–1012, 1999.
13. H. Murakami, Laminated Composite Plate Theory with Improved In-Plane Responses, *J. Appl. Mech.*, vol. 53, pp. 661–666, 1986.
14. E. I. Grigolyuk and G. M. Kulikov, Toward a Theory of Elastic Laminated Anisotropic Shells, *Soviet Physics Doklady*, vol. 29, pp. 344–345, 1984.
15. E. I. Grigolyuk and G. M. Kulikov, *Multilayered Reinforced Shells: Analysis of Pneumatic Tires*, Mashinostroyenie, Moscow, 1988 (in Russian).
16. G. M. Kulikov, Analysis of Initially Stressed Multilayered Shells, *Int. J. Solids Struct.*, vol. 38, pp. 4535–4555, 2001.
17. G. M. Kulikov, Non-Linear Analysis of Multilayered Shells under Initial Stress, *Int. J. Non-Linear Mech.*, vol. 36, pp. 323–334, 2001.
18. N. J. Pagano, Influence of Shear Coupling in Cylindrical Bending of Anisotropic Laminates, *J. Composite Mater.*, vol. 4, pp. 330–343, 1970.
19. T. J. R. Hughes and W. K. Liu, Nonlinear Finite Element Analysis of Shells. Part II: Two-Dimensional Shells, *Comput. Meth. Appl. Mech. Eng.*, vol. 27, pp. 167–182, 1981.
20. D. Lam, W. K. Liu, E. S. Law, and T. Belytschko, Resultant-Stress Degenerated-Shell Element, *Comput. Meth. Appl. Mech. Eng.*, vol. 55, pp. 259–300, 1986.
21. K. J. Bathe and E. N. Dvorkin, A Formulation of General Shell Elements—the Use of Mixed Interpolation of Tensorial Components, *Int. J. Numer. Meth. Eng.*, vol. 22, pp. 697–722, 1986.
22. J. C. Simo, D. D. Fox, and M. S. Rifai, On a Stress Resultant Geometrically Exact Shell Model. Part II: The Linear Theory; Computational Aspects, *Comput. Meth. Appl. Mech. Eng.*, vol. 73, pp. 53–92, 1989.
23. G. R. Heppler and J. S. Hansen, A Mindlin Element for Thick and Deep Shells, *Comput. Meth. Appl. Mech. Eng.*, vol. 54, pp. 21–47, 1986.
24. Y. Basar, Y. Ding, and R. Schultz, Refined Shear-Deformation Models for Composite Laminates with Finite Rotations, *Int. J. Solids Struct.*, vol. 30, pp. 2611–2638, 1993.
25. S. P. Timoshenko and J. N. Goodier, *Theory of Elasticity*, 3rd ed., McGraw-Hill, New- York, 1970.
26. R. H. MacNeal and R. L. Harder, A Proposed Standard Set of Problems to Test Finite Element Accuracy, *Finite Elements Anal. Des.*, vol. 1, pp. 3–20, 1985.